INSTRUMENTATION

Optimization of Analog-Circuit Motion Correction for Liver Scintigraphy

N. H. Baimel and M. J. Bronskill

The Ontario Cancer Institute, Toronto, Canada

Respiratory motion customarily degrades the resolution of a routine hepatic scintigram. We have analyzed four analog motion-correction methods and have measured their abilities to maintain good spatial resolution over a broad range of liver scintigraphy parameters. The analog circuit described can maintain the spatial resolution of the scintillation camera within 2 mm of the full width at half maximum of the stationary point-spread function. Experiments show that clinicians require about 50% greater film-density contrast to detect a 2-cm-diam. lesion if motion correction is not used. In 14% of the cases studied, the addition of a motion-corrected anterior view to the usual four-view liver study (performed without motion correction) resulted in a changed clinical interpretation. We conclude that analog motion correction should be provided in all scintillation cameras used for liver scintigraphy.

J Nucl Med 19: 1059–1066, 1978

As the spatial resolution of scintillation cameras continues to improve, respiratory motion presents a limitation of increasing importance to liver scintigraphy. The techniques that have been employed to reduce the degradation of spatial resolution due to respiratory motion can be divided into three categories:

1. Gating techniques (*1,2*);
2. Computer techniques (*3,4*); and
3. Analog-circuit techniques (*5,6*).

For routine clinical use, the analog-circuit technique is attractive because it avoids the expense and complexity of a dedicated computer and does not increase the time required for a liver study. Although several analog motion-correction circuits have been described (*5,6*), or advertised*, little work has been published to quantify their performance, thus permitting evaluation and comparison of various circuits.

We have analyzed several motion-correction methods to compare their abilities to maintain good spatial resolution over a broad range of clinical conditions encountered in liver scintigraphy. A circuit was designed to implement one such method, and experiments were performed to measure its capabilties. It is difficult, however, to relate objective parameters of motion correction (such as improved spatial resolution) to improved detection of focal lesions in liver scintigraphy. As a first step towards establishing such a relationship, we have determined the count-density contrast necessary for an observer to detect a single focal lesion with and without motion correction. Because this simple detection experiment is somewhat artificial compared with the clinical situation, we have also evaluated the clinical impact of a single motion-corrected anterior view on a routine four-view liver study, performed without motion correction, for a random series of patients.

Theoretical considerations. Analog motion correction is performed by using mathematical combinations of coordinate signals as an index of respiratory motion. The technique is illustrated in Fig. 1, where

Received Nov. 28, 1977; revision accepted March 27, 1978.

For reprints contact: M. J. Bronskill, Physics Div., Ontario Cancer Inst., 500 Sherbourne St., Toronto, Canada, M4X 1K9.

y_i is the y coordinate of an individual scintillation;
y_c is the signal corresponding to the position of the center of activity of the liver; and
y_i^{cor} is the y coordinate signal of a scintillation corrected for a displacement, y_c.

The displacement of the liver from the origin at any time can be approximated by averaging N consecutive y coordinate signals (i.e., $y_c \sim 1/N \sum_{i=1}^{N} y_i$). By subtracting the current center of activity, y_c, from each y coordinate signal, y_i, a corrected y coordinate signal, y_i^{cor} is derived, which is the corresponding coordinate in a stationary liver with center of activity at the origin. For this example it is assumed that translational motion occurs only in the y direction.

The above description of analog motion correction is oversimplified, and for a thorough analysis of the technique one must investigate both the mathematical combination of coordinate signals (algorithm) most effective in maintaining spatial resolution, and the best choice for N, the effective number of coordinate signals used to determine the position of the center of activity, y_c. Note that the choice of N may depend on the particular algorithm used, and that individual y coordinate signals, y_i, are not necessarily equally weighted in determining y_c.

An effective analog correction technique must maintain good spatial resolution over the complete range of respiratory parameters encountered in clinical liver scintigraphy. These parameters were measured for a group of twenty randomly selected patients and are listed in Table 1. The liver's respiratory excursion and frequency were determined with a circuit designed to measure y_c as a function of time. Its respiratory excursion in Table 1 was measured along the y (spinal) axis of the patient. Respiratory excursion along the x axis was measured to be less than 3 mm for all patients and was considered negligible. The plots of y_c as a function of time were close to sinusoidal, with no flattening of the peaks or valleys at extreme excursions. This suggests that there is little deformation of the liver due to respiratory motion, consistent with the assumption, made earlier, that degradation of spatial resolution is primarily due to translational motion along the patient's y axis.

Four analog correction techniques were analyzed for this range of parameters, with the position of the center of activity derived from:

1. A linear extrapolation of two consecutive determinations of the center of activity of the liver;
2. One previous determination of the center (centroid) of activity of the liver;

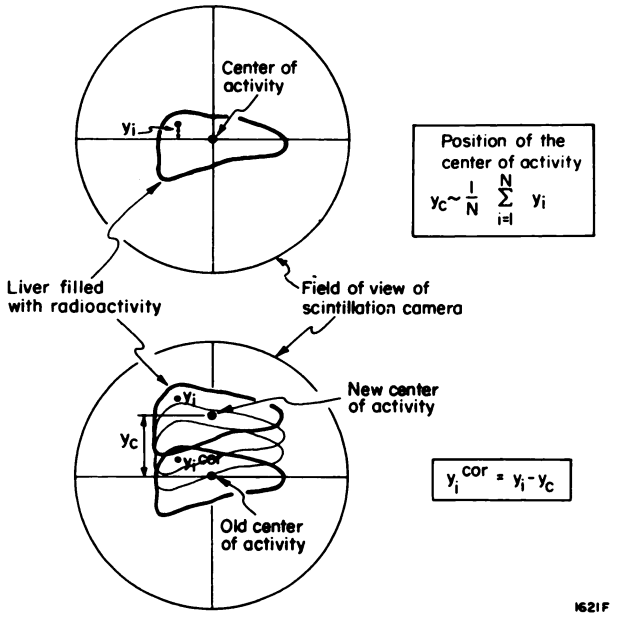

FIG. 1. General procedure for analog motion correction in liver scintigraphy. Symbols are defined in text.

3. A weighted interpolation of two consecutive determinations of the center of activity of the liver; and
4. An exponentially weighted determination of the center of activity of the liver.

To determine the ability of these techniques to maintain spatial resolution, we define the corrected point-spread function (CPSF) as the distribution of coordinates equivalent to a point source of activity in a motion-corrected image of an oscillating liver. The full width at half maximum (FWHM) of the CPSF was calculated for all four techniques as a function of the liver's respiratory excursion (see Fig. 2, numbered solid lines). An outline of the calculations for Algorithm 4 is given in the Appendix.

From Fig. 2 it is apparent that all four algorithms are effective in restoring spatial resolution for respiratory excursions greater than about 5 mm. Comparison of these algorithms in this format is valid because the choice for N was optimized for each technique individually, as discussed later in this sec-

TABLE 1. LIVER SCINTIGRAPHY PARAMETERS*

	Average	Range
Liver respiratory excursion cm, peak-to-peak	1.4	0.9–2.6
Respiratory frequency	15/min	10–20/min
Count rate sec^{-1}	5,500	4,500–6,500

* Measured for 20 patients, anterior view only.

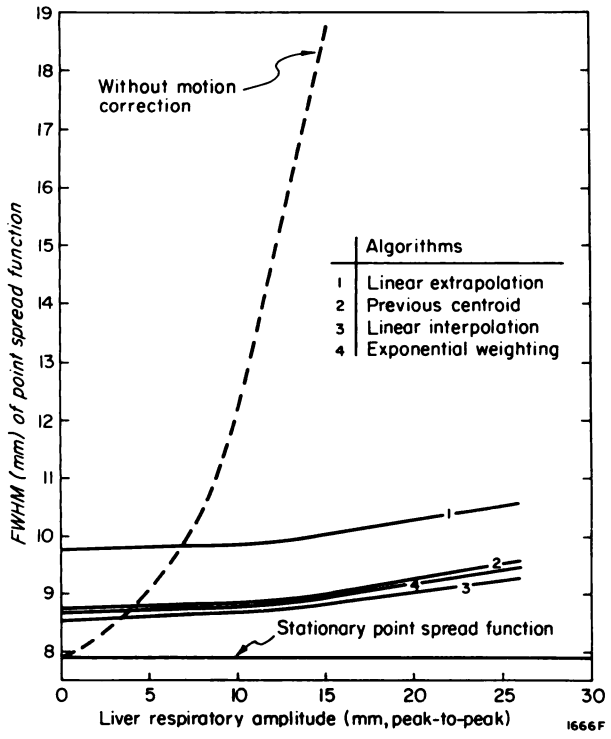

FIG. 2. Theoretical comparison of motion-correction algorithms as a function of liver respiratory motion, assuming a correction signal derived from a liver phantom of average dimensions, translated in simple harmonic motion with frequency 15/min, and a count rate 5,400/sec. Calculations assumed a scintillation camera with a FWHM of 7.9 mm for the stationary point-spread function.

tion. Algorithms 2, 3, and 4 are clearly more effective than Algorithm 1, a result that also holds for varying respiratory frequencies and count rates. We chose to implement Algorithm 4 because its equivalent electronic circuit was simpler and more stable than those of Algorithms 2 and 3.

The block diagram of the analog circuit is shown in Fig. 3. The design of this circuit is similar to the circuits introduced by Hoffer et al. (*5*) and Elings et al. (*6*). For each count accepted by the scintillation camera, the y coordinate signal is sampled and then held until the next accepted count. In our circuit, a 500-kHz clock switches the y coordinate signal into a "leaky" integrator, a feature that enables circuit calibration to be independent of count rate. The integrator is "leaky" because the charge stored on the capacitor C_1 is lost through the resistor R at a rate determined by the time constant $T = RC_1$. Thus, y coordinates reaching the integrator are weighted exponentially, with those occurring most recently in time having the greatest weight. The leaky integrator's time constant, T, effectively determines N, the number of y coordinate signals used to determine y_c. The actual correction signal, y_{cor}, lags behind the true position of the center of activity, y_c. This lag, or phase shift, is also dependent on T.

The optimum choice for N must also take into account the wide range of parameters given in Table 1. This was done for all four algorithms and is demonstrated for Algorithm 4 in Fig. 4, where the FWHM of the CPSF is shown as a function of T. Note that for each set of respiratory parameters, there is an optimum time constant, and the practical choice for T is a compromise. A small time constant implies that few y coordinate signals are used to derive y_{cor}; thus there is a large statistical error associated with the correction signal. A large time constant achieves a smaller statistical error in the correction signal, but at the expense of greater phase lag between the correction signal and the current position of the center of activity. From Fig. 4, a compromise time constant of 0.12 sec can be chosen. For each of the seven curves, the FWHM of the CPSF at $T = 0.12$ sec lies within 0.2 mm of the minimum *for that curve.*

METHODS AND RESULTS

Spatial resolution. The performance of the circuit implementing Algorithm 4 was tested to verify that motion correction could achieve the predicted improvements in spatial resolution. A point source of I-131, and a liver phantom of average size (17 cm $\times$ 17 cm) containing Tc-99m, were oscillated in linear simple harmonic motion along the y axis of

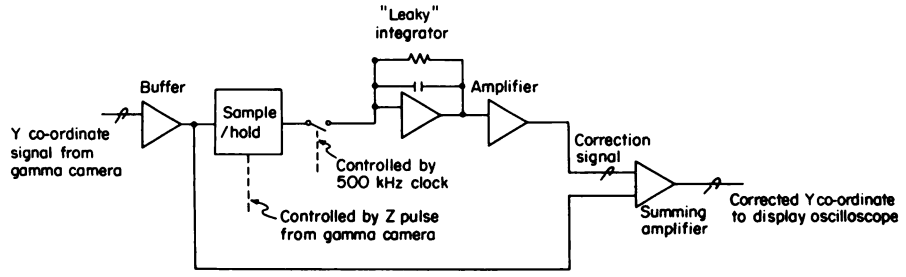

FIG. 3. Block diagram of motion-correction circuit implementing Algorithm 4. Correction signal from leaky integrator is amplified, then subtracted from each y coordinate in the summing amplifier.

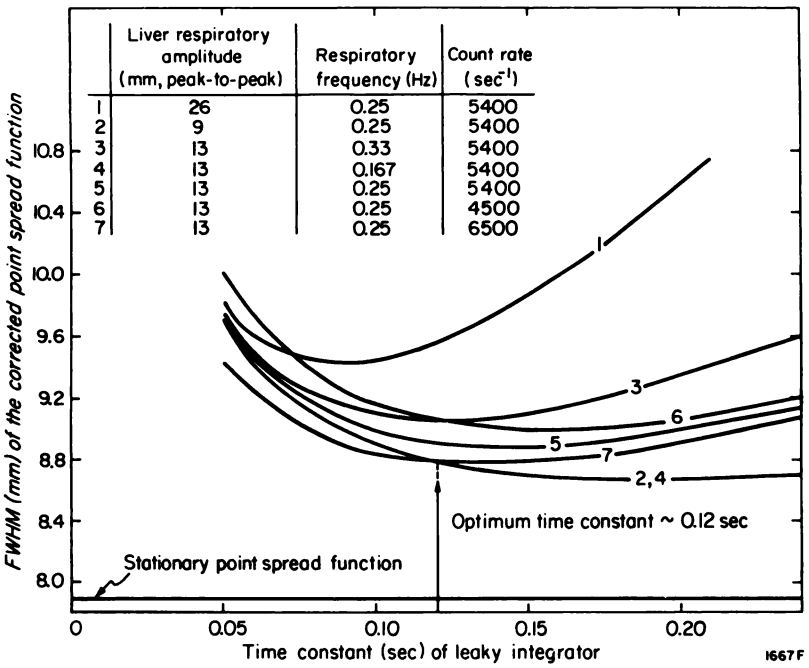

FIG. 4. Graphical determination of optimum time constant for "leaky" integrator. Curve 5 was based on average parameters of Table 1; the other six curves for extremes of Table 1. Calculations assumed a scintillation camera with stationary point-spread function of 7.9 mm, FWHM.

the detector of a scintillation camera. Energy signals from the camera were used to separate the two radionuclides and a correction signal, derived with y coordinate signals from the liver phantom, was used to correct the motion of the point source. For the complete range of parameters of liver scintigraphy in Table 1, the FWHM of the corrected and uncorrected point-spread functions were measured, and these results, along with the FWHM of the CPSF calculated for these same parameters, are shown in Figs. 5 and 6. There is substantial improvement in spatial resolution when the motion-correction circuit is used. Over the full range of liver scintigraphy parameters of Table 1, the FWHM of the CPSF is less than 2 mm wider than the FWHM of the *stationary* point-spread function. The calculated FWHM of the CPSF is slightly smaller than the measured FWHM of the CPSF, and this difference of ~0.3 mm is essentially constant over the range of liver-scintigraphy parameters.

Observer response. Although analog motion correction can be formulated theoretically and tested experimentally, the performance of an observer in detecting focal lesions with motion correction must be evaluated to determine the clinical significance of motion correction. To this end, an experiment with an oscillating liver phantom was performed to determine the count-density contrast necessary for an observer to detect a single focal lesion with and without motion correction. The liver phantom was constructed so that its image resembled the distribution of activity seen in a normal anterior liver scinti-

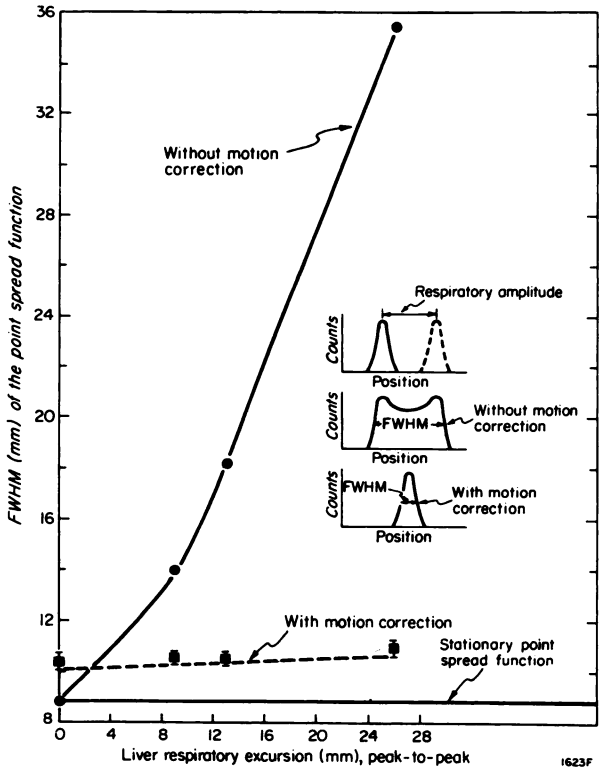

FIG. 5. Improvement in spatial resolution of Picker Dynacamera 2C camera due to analog motion correction, plotted as a function of the liver's respiratory motion. Correction signal derived from liver phantom of average dimensions, moved in simple harmonic motion with frequency of 15/min, and count rate 5,700/sec. Solid line was measured without motion correction. Dashed line was calculated and the points (■) measured under motion correction. Error bars represent uncertainty in measuring FWHM due to collimator septal penetration and variation from position to position on detector face.

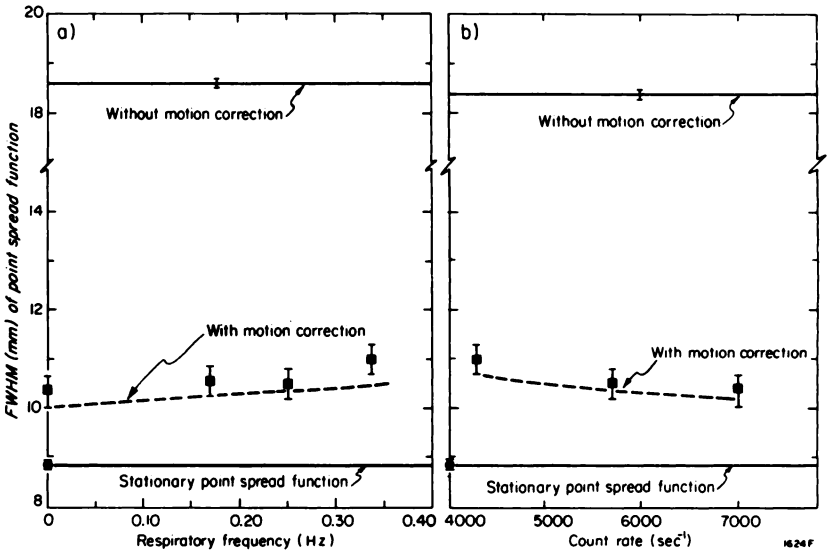

FIG. 6. Improvement in spatial resolution of Picker Dynacamera 2C camera due to analog motion correction, as a function of (a) respiratory frequency and (b) count rate. Correction signal derived from liver phantom of average dimensions, moved in simple harmonic motion with amplitude 1.3 cm (peak-to-peak). In (a) count rate was 5,700/sec, and in (b) respiratory frequency was 15/min. Dashed lines were calculated and points (■) measured with motion correction. Error bars represent uncertainty due to septal penetration and local variation in FWHM of PSF.

gram. The focal lesion was simulated using various thicknesses of aluminum disks, 2 cm in diam., placed on the surface of the liver phantom, 3 cm from the collimator face of a scintillation camera. To measure the response of an observer to the image of this test pattern, we adopted a procedure similar to the method of constant stimuli (7). Five different thicknesses of aluminum disk were used, producing a range of lesion images from the barely perceptible to the clearly visible. The aluminum disks were placed on the liver phantom in five different locations of similar count density. Three sets of images were produced under the conditions of: motion with correction, motion without correction, and no motion. The liver-scintigraphy parameters used to produce these sets of images were the average parameters from Table 1, with a larger-than-average respiratory amplitude of 1.9 cm. For each of these three conditions, two images were produced for each lesion contrast and each lesion location. Four images were produced with no lesion present.

All images were exposed to a maximum count density of 4,000 c/cm^2, yielding a peak film density of 1.3 $\pm$ 0.07, including base plus fog. These parameters are used routinely for liver scintigraphy in our department. The count-density contrast of the five aluminum disk thicknesses was determined using a computer† interfaced to the scintillation camera. In this work the count-density contrast is defined as the magnitude of the difference in count density between the lesion and its surrounding area, divided by the count density of the surrounding area. For the five thicknesses of aluminum disk used, count-density contrast increased linearly with disk thickness, each 1.07-mm disk of aluminum producing an increase of 0.015 in count-density contrast. To determine whether film characteristics affect observer performance in detecting focal lesions, all images were produced on two kinds of 70-mm film: Kodak PF and Dupont SF2. Previous experience indicated that these two film types had substantially different characteristics and could, therefore, provide an indication of the influence of film type on this kind of study. Overall, 324 images were produced.

The images were randomized and then examined at one sitting by three experienced nuclear medicine clinicians. For each image, the clinician was asked to determine whether a single lesion was present. If he were certain that a lesion was present, he was asked to indicate its position in the phantom. Because liver scintigraphy yields a significant number of equivocal images, the clinician was also allowed to indicate any area on an image that he considered suspicious but not definitely abnormal.

Figure 7 shows the cumulative visual response of the three clinicians for all 324 images (excluding suspicious areas). True-positive percentage is plotted as a function of aluminum attenuator thickness (or count-density contrast). The response curves determined under the conditions of motion correction and no motion are essentially identical. For motion without correction, a considerable increase in contrast is required to permit detection of the lesion. For example, approximately 50% greater count-density contrast is required to obtain a 90% true-positive rate under the condition of motion without correction than under the other two conditions.

In Fig. 8 the visual responses for the three clinicians are separated by film type for both motion with correction and no motion. For a 90% true-positive result, the clinicians require about 35% more count-density contrast to identify the lesions

with Kodak PF film than with Dupont SF2 film (i.e., approximately 7 *vs* 5.2 disk thicknesses, respectively). This result can be understood by considering the film density contrast characteristics of the two film types.

Figure 9 shows *linear* plots of exposure against film density, measured for both films using a Co-57 flood field exposed for various lengths of time. For the areas where the lesions were placed, which corresponded to a film density of ~1.15, the slopes of the curves were determined to be 0.63 for PF film and 0.85 for SF2 film. Seven attenuator thicknesses result in a film-density contrast of 0.066 ($7 \times 0.015 \times 0.63$) for PF film and 5.2 attenuator thicknesses result in a film-density contrast of 0.066 ($5.2 \times 0.015 \times 0.85$) for SF2 film. The clinicans respond to film-density contrast, not to count-density contrast.

Clinical evaluation. To evaluate the impact of analog motion correction in routine clinical use, in 52 patients a motion-corrected anterior view was added to our usual four-view liver study performed without motion correction. The nuclear medicine clinician was asked to read the four uncorrected views and to reach an initial interpretation. The motion-corrected view was then read and a final interpretation reached, thus permitting any influence made by the additional image to be evaluated. In 19 cases the clinical interpretation was influenced but not changed by the addition of the motion-corrected image. In seven out of 52 cases (14%) the clinical interpretation was changed. In five of these cases, the extra, motion-corrected image enabled the interpretation to be changed from suspicious or equivocal to normal or abnormal. In the other two cases, an initial interpretation of normal or enlarged was altered to suspicious.

DISCUSSION

We have been able to model the performance and compare the capabilities of four analog motion-correction algorithms. The exponentially weighted algorithm has been implemented as a simple electronic circuit. A dual-nuclide experiment was used to confirm the ability of this circuit to maintain the FWHM of the CPSF within 2 mm of the stationary PSF over a broad range of practical liver-scintigraphy parameters. The measured FWHM of the CPSF was approximately 0.3 mm greater than the calculated FWHM, a discrepancy that we attribute to broadening of the stationary PSF by septal penetration of the low-energy collimator by I-131 radiations. Basically, we consider the good agreement between theory and experiment to validate the mathematical approach and thus permit easy comparison of the four algorithms.

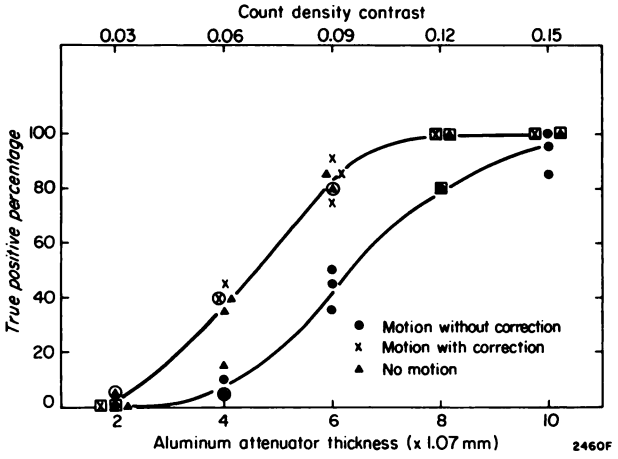

FIG. 7. Visual response curves of three nuclear medicine clinicians. Results for both film types are combined. Open circles around symbols indicate two identical clinician responses; open squares around symbols indicate three coincident clinician responses.

The visual response of clinicians in the detection of the 2-cm lesion indicates that approximately 50% greater count-density contrast is required to detect the lesion if motion correction is not used. The fact that the clinicians did equally well with motion-corrected images and images of a stationary phantom confirms that there was little degradation of spatial resolution when this motion-correction circuit was used. This result is not surprising when one considers that the equivalent FWHM of the PSF at a lesion position 3 cm from the collimator face is about 10.3 mm, and our calculations indicate that with this motion-correction circuit, the CPSF would

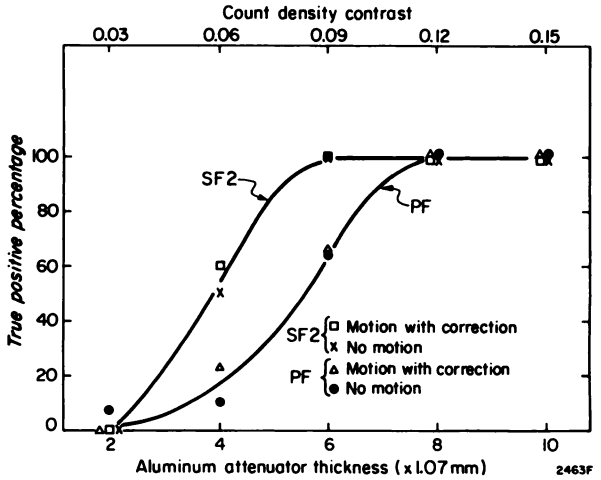

FIG. 8. Visual response curves of clinicians for images produced under the conditions of motion with correction, and with no motion. Film types tested are indicated.

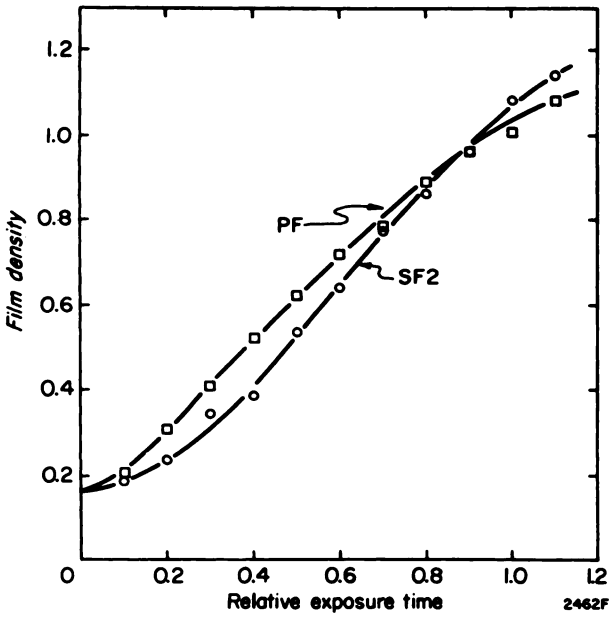

FIG. 9. Linear plots of exposure versus film density for PF and SF2 films. PF film required approximately 1.5 times the exposure of SF2 film to reach film density of 1.0 (including base plus fog).

have an FWHM of 11.1 mm under the conditions of the study. Our simple test of adding a motion-corrected anterior view to the four-view clinical liver study indicates that motion correction is most likely to clarify the interpretation of equivocal or suspicious studies. This result could be of considerable benefit: in our department, 256 of 1973 liver studies (13%) have been read as equivocal or suspicious during 1975 and 1976. Motion correction also yields a more accurate y dimension for estimations of liver size, although it should be noted that the present "normal" y dimension of 17 cm effectively incorporates about 1.1 cm of motion, as indicated by Table 1.

The influence of different film characteristics on lesion detection is a well-known but poorly quantified phenomenon. The apparent superiority of SF2 film in this lesion-detection test is readily understood in terms of the *linear* plots of exposure against film density for PF and SF2 films. The lesion was placed in an area of film density 1.15. *In this density region*, a small decrease in local count density produces a change in film-density that is larger for SF2 than for PF. Of the total of 14 false suspicious areas indicated by the clinicians, seven were indicated for each film type. Thus there is no apparent increase in false positives or over-reading associated with SF2 film in this test. We believe that SF2 is a better film than the PF for the detection of focal lesions in liver scintigraphy.

Several additional factors should be considered in the application of this motion-correction technique. A large-sized distribution of activity in the y-direction field of view of the scintillation camera degrades the performance of all analog motion-correction techniques. Inclusion of the spleen in the field of view, however, does not usually increase the y direction distribution of activity. Moreover, inclusion of some liver in an image of the spleen is probably beneficial under motion correction because it increases the count rate, and our measurements indicate that liver and spleen usually exhibit the same respiratory amplitude. We do not observe decreased respiratory amplitude with patients in the prone position.

With this technique, optimum motion correction is achieved when the average position of the center of activity of the liver lies near the origin of the detector (see Appendix, Eq. 2). This is not a limitation, because the best uniformity and spatial resolution of the detector are usually obtained in this area. If motion correction is also applied to the persistence oscilloscope, it is straightforward to test on the persistence scope that the image does not shift when motion correction is activated. The choice of time constant for the circuit described in this paper is optimized for the range of parameters of Table 1 and a scintillation camera with a PSF of 7.9 mm FWHM. These factors do vary (depending on injected activity, collimator sensitity, scintillation camera, patient size, etc.), so the time constant appropriate for a specific application should be estimated using the Appendix.

Our experiments, both clinical and physical, indicate that analog motion correction is very effective in maintaining good spatial resolution, and we believe this feature should be provided in all scintillation cameras used for liver scintigraphy.

APPENDIX

This appendix gives a simplified derivation of an equation that allows the calculation of the FWHM of the CPSF for a scintillation camera with a known FWHM of the stationary PSF, over a full range of liver scintigraphy parameters. There are three major factors that contribute to the FWHM of the CPSF:

1. The stationary PSF of the scintillation camera;
2. The statistical error associated with the correction signal; and
3. The phase shift between the correction signal and the current position of the center of activity.

Stationary PSF. This can be closely approximated by a normal distribution of standard deviation σ_p. The FWHM of the stationary PSF is 2.354 σ_p.

Statistical error. The statistical error can be thought of as the distribution of y_{cor} signals that would be observed in the case of a stationary liver. Ideally y_{cor} should be the mean, μ, of the distribution of y coordinates. The y_{cor} signal is derived, however, with a finite number N of randomly occurring y coordinate signals. In the circuit implemented in this work, there is an additional uncertainty introduced by the 500-kHz clock, which gates each y coordinate into the leaky integrator a random number of times. An exponential factor determined by the integrator time constant, T, also weights each coordinate in time.

If the distribution of y coordinates is characterized by a standard deviation σ_y and a mean μ, it can be shown that the distribution of signals to the integrator is of mean μ and standard deviation $\sqrt{2(\sigma_y^2 + \mu^2)}$. When the exponential-weighting characteristics of the integrator are taken into account, the standard deviation of the statistical-error distribution is given by

$$\sigma_s^2 = \frac{\sigma_y^2 + \mu^2}{CT}, \quad (1)$$

where C is the count rate (sec^{-1}) and T is the integrator time constant (sec). Obviously the standard deviation of the statistical error can be minimized for any σ_y if the liver is positioned in the scintillation camera field of view such that $\mu = 0$. In this case,

$$\sigma_s = \frac{\sigma_y}{\sqrt{CT}}. \quad (2)$$

Phase error. The phase error is due to the lag between the correction signal and the true position of the center of activity. Assume that the center of activity moves in simple harmonic motion given by

$$y_c(t) = \frac{A \sin(2\pi ft)}{2}, \quad (3)$$

where A is the peak-to-peak liver respiratory excursion (cm) and f is the respiratory frequency (Hz). The phase error, y_{ph}, is defined as the difference between $y_{cor}(t)$ and $y_c(t)$, and varies with time. This phase error can be defined mathematically as a distribution of mean zero whose standard deviation σ_{ph} is given by

$$\sigma_{ph} = \frac{A\pi ft}{\sqrt{2 + 2(2\pi fT)^2}}. \quad (4)$$

Motion-corrected PSF. The error in the positioning of an individual y coordinate through this motion-correction circuit can now be determined from the standard deviations of three independent distributions: the stationary point-spread function (σ_p), the statistical error (σ_s), and the phase error (σ_{ph}). Measurement has confirmed that the CPSF has a very nearly normal distribution, thus the FWHM of the CPSF is given by

$$\begin{aligned} FWHM &= 2.354\sqrt{\sigma_p^2 + \sigma_s^2 + \sigma_{ph}^2} \\ &= 2.354\sqrt{\sigma_p^2 + \frac{\sigma_y^2}{CT} + \frac{(A\pi ft)^2}{2 + 2(2\pi ft)^2}}. \end{aligned} \quad (5)$$

Equation 5 can be used to calculate the performance of this circuit for any scintillation camera whose stationary PSF is known, for a broad range of liver-scintigraphy parameters.

FOOTNOTES

* Matrix Instruments, Northvale, N.J. and Searle Diagnostics Inc., Des Plaines, Ill.

† PDP-11/40, Digital Equipment Corp., Maynard, Mass.

REFERENCES

1. SMOAK WM, SMITH EM, KENNY PJ: Reduction of physiologic degradation in imaging the liver. *J Nucl Med* 12: 119–122, 1971

2. DELAND FH, MAUDERLI W: Gating mechanisms for motion-free liver and lung scintigraphy. *J Nucl Med* 13: 939–941, 1972

3. OPPENHEIM BE: A method using a digital computer for reducing respiratory artifact on liver scans with a camera. *J Nucl Med* 12: 625–628, 1971

4. SCHMIDLIN P: Development and comparison of computer methods for organ motion correction in scintigraphy. *Phys Med Biol* 20: 465–476, 1975

5. HOFFER PB, OPPENHEIM BE, STERLING ML, et al: A simple device for reducing motion artifacts in gamma camera images. *Radiology* 103: 199–200, 1972

6. ELINGS VB, MARTIN CB, POLLACK IG, et al: Electronic device corrects for motion in gamma camera images. *J Nucl Med* 15: 36–37, 1974

7. SHARP PF: Psychophysical assessment of the performance of clinical radioisotope imaging devices. In *Medical Images: Formation, Perception and Measurement*, George A. Hay, editor, London, The Institute of Physics, John Wiley and Sons, 1976